Behavioral/Cognitive

Exploring Information Flow from Posteromedial Cortex during Visuospatial Working Memory: A Magnetoencephalography Study

Erin Goddard,[1] Erika W. Contini,[2] and Muireann Irish[3]
[1]School of Psychology, University of New South Wales, Sydney, NSW 2052, Australia, [2]Department of Cognitive Science, Macquarie University, Macquarie Park, NSW 2109, Australia, and [3]University of Sydney, School of Psychology and Brain & Mind Centre, Sydney, NSW 2050, Australia

The posteromedial cortex (PMC) is a major hub of the brain's default mode network, and is implicated in a broad range of internally driven cognitions, including visuospatial working memory. However, its precise contribution to these cognitive processes remains unclear. Using MEG, we measured PMC activity in healthy human participants (young adults of both sexes) while they performed a visuospatial working memory task. Multivariate pattern classification analyses revealed stimulus-related information during encoding and retrieval in a set of *a priori* defined cortical ROIs, including prefrontal, occipital, and ventrotemporal cortices, in addition to PMC. We measured the extent to which this stimulus information was exchanged between areas in an information flow analysis, measuring Granger-causal relationships between areas over time. Consistent with the visual nature of the task, information from occipital cortex shaped other regions across most epochs. However, the PMC shaped object representations in occipital and prefrontal cortices during visuospatial working memory, influencing occipital cortex during retrieval and PFC across all task epochs. Our findings are consistent with a proposed role for the PMC in the representation of internal content, including remembered information, and in the comparison of external stimuli with remembered material.

Key words: **episodic memory; information flow analysis; MEG; posterior cingulate cortex; visuospatial memory**

Significance Statement

The human brain operates as a collection of highly interconnected regions. Mapping the function of this interconnectivity, as well as the specializations within different regions, is central to understanding the neural processes underlying cognition. The posteromedial cortex (PMC) is a highly connected cortical region, implicated in visuospatial working memory, although its precise contribution remains unclear. We measured the activity of PMC during a visuospatial working memory task, testing how different regions represented the stimuli, and whether these representations were driven by other cortical regions. We found that PMC influenced stimulus information in other regions across all task phases, suggesting that PMC plays a key role in shaping stimulus representations during visuospatial working memory.

Introduction

The posteromedial cortex (PMC) encompasses the posterior cingulate cortex and precuneus, and is widely held to support a variety of internally driven forms of cognition (Andrews-Hanna, 2012). As a hub of the brain's default mode network, the PMC demonstrates extensive connections with the medial temporal lobe, as well as frontoparietal brain regions associated with cognitive control (Leech et al., 2012). fMRI studies delineating subdivisions within the PMC point to distinct patterns of connectivity with other areas during the resting state (Margulies et al., 2009; Bzdok et al., 2015; Kernbach et al., 2018; Khan et al., 2020) as well as divergent task-related functional connectivity as task difficulty increases (Leech et al., 2011, 2012; Bzdok et al., 2015). Given the richness of these connections, and the heterogeneity of PMC subregions (Margulies et al., 2009; Leech et al., 2011), the PMC is, perhaps unsurprisingly, implicated across a diverse range of cognitive functions. Such functions include self-referential processing, visual imagery, translating egocentric to allocentric representations, and modulating internally versus externally directed forms of cognition (for review, see Bzdok et al., 2015).

Received Oct. 24, 2021; revised June 6, 2022; accepted June 7, 2022.

Author contributions: E.G., E.W.C., and M.I. designed research; E.G. analyzed data; E.G., E.W.C., and M.I. edited the paper; E.G. and M.I. wrote the paper; E.W.C. performed research.

This work was supported by Australian Research Council (ARC) Center of Excellence in Cognition and its Disorders (CE110001021). E.G. was supported in part by ARC DECRA Fellowship (DE200100139). M.I. was supported by ARC Future Fellowship (FT160100096) and ARC Discovery Project (DP180101548). This research includes computations using the computational cluster Katana supported by Research Technology Services at University of New South Wales Sydney (https://doi.org/10.26190/669x-a286). We thank Elizabeth Magdas for assistance with MEG data collection; and Nicole Kochan for supplying the visual stimuli.

The authors declare no competing financial interests.

Correspondence should be addressed to Erin Goddard at erin.goddard@unsw.edu.au.

https://doi.org/10.1523/JNEUROSCI.2129-21.2022

Despite no direct connections to sensory cortex, the PMC appears ideally positioned to receive converging sensory-perceptual input, largely visual in nature, to support the integration of visuospatial information (Conti and Irish, 2021). These representations can be maintained online and operated on (i.e., working memory) (Kravitz et al., 2011; Hunsaker and Kesner, 2018), or integrated into contextually rich reconstructions of past experiences (i.e., episodic memory) (Lega et al., 2017; Natu et al., 2019). A consistent finding in the memory literature is that of significant PMC activation during tasks that require the reinstatement of contextual information (Bird et al., 2015). Moreover, activity within PMC subregions has been shown to parametrically scale with the vividness of retrieved information, suggesting an important role in memory phenomenology, while other subregions of PMC have been suggested to represent unique configurations of event features (Cooper and Ritchey, 2019). Collectively, these studies indicate a central role for the PMC in representing and integrating different types of information in the service of memory (for review, see Ritchey and Cooper, 2020).

Studies exploring the evolving time course of PMC activity across task phases have consistently demonstrated an "encoding/retrieval flip," where successful remembering is associated with attenuated PMC activity during encoding but increased activity during retrieval (Daselaar et al., 2004, 2009; Huijbers et al., 2012, 2013). Importantly, by comparing the locations of voxels driving associations between performance and attenuation, then facilitation, Vannini et al. (2011) demonstrated that the same PMC subregions modulate the encoding/retrieval flip. Patterns of functional connectivity with PMC have also been shown to evolve across memory task phases (e.g., Piccoli et al., 2015). For example, theta phase medial temporal lobe-neocortical synchrony reliably predicts the degree of visual imagery recollected during autobiographical memory retrieval, correlating specifically with activity in the precuneus (Fuentemilla et al., 2014), resonating with the proposed role of the PMC in the reinstatement of visuospatial sensory-perceptual details. Thus, while there is evidence to suggest information transfer between the PMC and other brain regions during memory performance (Canolty et al., 2006; Fell and Axmacher, 2011; Sauseng et al., 2019), the direction of this information exchange remains poorly understood.

The objective of this study was to leverage the temporal precision of MEG to establish the patterns of information flow between the PMC and other brain regions during visuospatial working memory performance. We used a novel measure of Granger-causal information exchange to test for evidence that PMC encodes stimulus attributes within different task phases and to determine whether any such information is transferred from the PMC to other brain regions. We predicted that, if connectivity between PMC and other regions reflects information exchange that is crucial for memory performance, we should find evidence that the PMC encodes the remembered stimulus and drives the encoding of this information in other regions.

Materials and Methods

Participants. We collected psychophysical, MEG and MRI data from 12 participants (10 female, 2 male, age 19-31 years, mean = 23.8 years). Each participant completed the psychophysical experiment in a 1 h session, followed a week later by the MEG experiment in a 2 h session. The anatomic MRI images were acquired in a half hour session on a separate day. One participant withdrew from the MEG study early because of a headache, so their data were excluded. All participants were healthy with no history of neurologic and/or psychiatric disorders and provided informed consent. Each participant had normal or corrected-to-normal visual acuity. Participant recruitment and experiments were conducted with the approval of the Macquarie University Human Research Ethics Committee, and in accordance with the Declaration of Helsinki.

Display apparatus and setup. Visual stimuli were presented using MATLAB (version R2014b) and routines from Psychtoolbox (Brainard, 1997; Pelli, 1997; Kleiner et al., 2007).

During MEG sessions, stimuli were projected through a customized window by an InFocus IN5108 LCD back-projection system (InFocus) located outside the Faraday shield, onto a screen located above the participant, with a display width of 12 degrees visual angle. Participants, lying supine, viewed the screen from 113 cm.

For the psychophysical experiment, stimuli were displayed on a Dell OptiPlex 9010 desktop computer driving an AMD Radeon HD 7570 graphics card to draw stimuli to a 60×33 cm Samsung SyncMaster SA950 Full HD 3D LED monitor, refreshed at 120 Hz. Experiments took place in a darkened room, and participants were seated and viewed the screen from a distance of 64 cm.

Visual stimuli and task. During the psychophysical and MEG sessions participants completed a visuospatial working memory task. We based the task and stimuli on a working memory challenge task used previously (Kochan et al., 2010, 2011). For our task, we used 8 of the abstract pattern images used in previous work (Fig. 1*A*). Each encoding and retrieval stimulus comprised one of these 8 images, at one of 9 locations (Fig. 1*B*). Each image was a square, 2.5 degrees visual angle in diameter, and each of the 9 locations was centered on a position 4 degrees visual angle from the center of the screen. A dark gray cross (see Fig. 1, width 1 degree) was always present at the center of the screen. All images were presented on a background of mean gray.

Every trial followed the sequence illustrated in Figure 1*C*. During encoding, four stimuli were presented, sequentially, with the same duration. The encoding stimuli were always four different images, at four different locations, and the participant was required to remember these four conjunctions of image identity and location. Following the encoding stimuli, dynamic white noise was presented for 800 ms (the maintenance period): the noise pattern was 20% contrast, centered on mean gray, updated at 120 Hz. We included dynamic noise during maintenance to reduce any visual afterimages caused by the encoding stimuli. After the maintenance period, a retrieval stimulus was presented, and participants indicated whether the retrieval stimulus was included in the encoding stimulus set for that trial. Following their response (via button press), participants received feedback: the fixation cross changed to green if they were correct and red if incorrect. After 200 ms of feedback, the fixation cross returned to dark gray and, after a variable intertrial interval of 300–800 ms (randomly varied across trials), the next trial began. The buttons used to respond target present/absent were swapped on each block.

Participants completed the task in blocks of 72 trials. To aid with the classifier analysis based on MEG signals (below), the stimuli used for each encoding stimulus was fully counterbalanced within each block. The 8 images at 9 locations gave 72 unique stimuli, and for every block of trials these 72 stimuli were used once each as the first, second, third, and fourth encoding stimuli. Sets of encoding stimuli were chosen so that they always contained four different images at four different locations, with no repeated images or locations. We preallocated half of these trials, randomly selected, to be "target present" trials, and the remainder to be "target absent" trials. For each trial, we selected a retrieval stimulus according to whether it was designated a "target present" trial (retrieval stimulus was one of the encoding stimuli) or a "target absent" trial (retrieval stimulus was not included during encoding). Unlike the encoding stimuli, the retrieval stimuli did not necessarily contain each of the 72 unique stimuli on every block, but all images and locations were used an equal number of times across the block.

We used the initial psychophysical session to both train participants on the task and to calibrate the task difficulty according to their performance. During the psychophysical session, the duration of the encoding and retrieval stimuli were varied across trials. On each trial, the encoding stimuli each had the same duration, and the retrieval stimulus was twice as long as this. Across each block, a range of 9 durations were used. Each

participant completed four initial training blocks, where encoding durations were 150–400 ms. We used each participant's behavior on the first four training blocks to choose a smaller range of durations for a second set of four task blocks. Data were used from this second set of four blocks to estimate the duration at which each participant reached 75% correct task performance. Sample data from 1 participant are shown in Figure 2*A*. For each participant, we fit their data with a sigmoidal function (Eq. 1), where proportion correct (P) varied with encoding duration *(10)* according to an intercept parameter (α, defining the duration, x, where $p = 0.75$), a slope parameter (β), and a lapse rate (r), according to the following:

$$P = 0.5 + 0.5 * (r/2 + (1 - r/2). \\ /(1 + e^{-(x-\alpha)./\beta}) \quad (1)$$

We found the best fitting function (shown in red in Fig. 2*A*) using the MATLAB function *nlinfit*. Based on this psychophysical data, we chose a single encoding stimulus duration for each participant for their MEG session, aiming for overall performance of ~75% correct. This target was chosen to ensure that no participant was at ceiling or floor task performance, and to make the task sufficiently challenging for each participant, since the results of Kochan et al. (2011) suggest that PMC is particularly involved in demanding visuospatial working memory challenges. During the MEG session, each participant completed 8 blocks of trials with this single encoding stimulus duration, and a retrieval stimulus duration of twice this value. The durations used for each participant, and their overall performance across the MEG session, are shown in Figure 2*B*.

MEG and MRI scanning protocols. MEG data were collected with a whole-head MEG system (model PQ1160R-N2, KIT) at Macquarie University consisting of 160 coaxial first-order gradiometers with a 50 mm baseline (Kado et al., 1999; Uehara et al., 2003). Before MEG measurements, five marker coils were placed on the participant's head. Marker positions, nasion, left and right preauricular points, and participant head shape were recorded with a pen digitizer (Polhemus Fastrack), using a minimum of 2000 points.

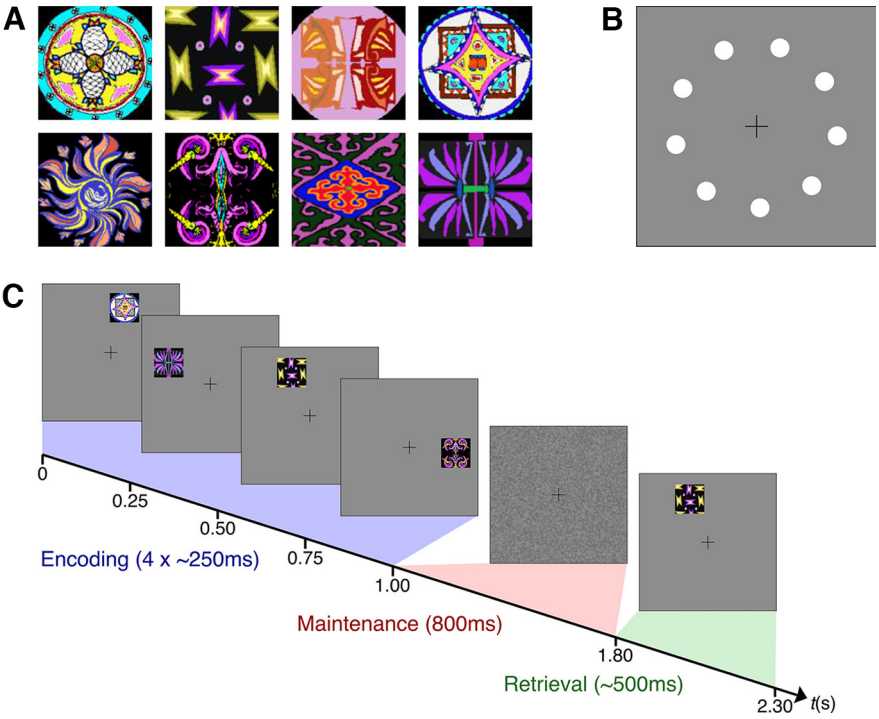

Figure 1. Stimuli and participant's task. In the visuospatial memory task, each stimulus was 1 of 8 abstract images (***A***) at 1 of 9 locations (***B***). On each trial, the participant was presented with 4 stimuli, serially presented, that were to be encoded in memory, followed by a dynamic noise screen for 800 ms (maintenance period) and then a single retrieval stimulus (***C***). The participant then responded via keypress whether the retrieval stimulus was present in the encoding stimulus set.

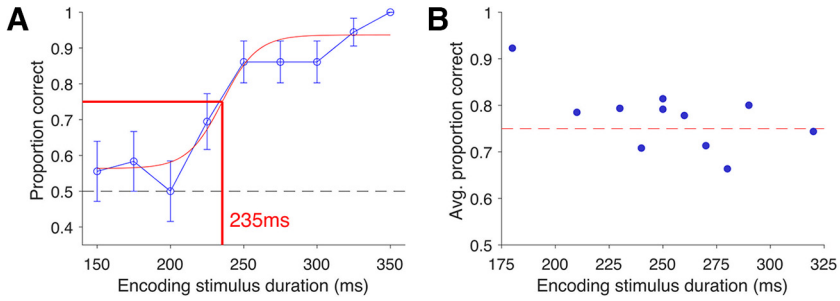

Figure 2. Behavioral performance. ***A***, Illustration of a single participant's data (blue line) with fitted psychometric function, showing fitted point of 75% correct (235 ms). Error bars indicate 95% CIs on the average performance across trials. ***B***, Each participant's performance in the MEG experiment against the encoding stimulus duration. Red dashed line indicates target value of 75% correct.

Each participant's MEG data were collected in a single session of ~90 min, at a sampling frequency of 1000 Hz. On each trial, participants responded using a Fiber Optic Response Pad (Current Designs).

MRI took place at the Macquarie University Hospital on a 3T Siemens Verio system. We acquired 3D T1-weighted images using an MP-RAGE sequence (slice thickness 1.0 mm, resolution 1.0 × 1.0 mm).

MEG data analysis: source reconstruction. The automatic segmentation processes from Freesurfer 6.0 (Dale et al., 1999; Fischl et al., 1999) was applied to each participant's structural MR to define their gray/white matter and pial/gray matter boundaries. Brainstorm (neuroimage.usc.edu/brainstorm, January 2019 version) (Tadel et al., 2011) was used to preprocess the MEG signals and perform source reconstruction. We imported the anatomic images and Freesurfer segmentations and defined head models based on each participant's pial/gray boundary (cortical surface). We aligned MEG datasets to the head model by aligning the anatomy based on the MRI to the recorded nasion, preauricular points, and head shape data from the MEG session. We generated a forward model for each of the 8 blocks of trials by applying a multiple spheres model (Huang et al., 1999) to their cortical surface at the measured head location during the block.

MEG data were preprocessed in Brainstorm with notch filtering (50, 100, and 150 Hz), followed by bandpass filtering (0.2–200 Hz). Cardiac and eye blink artifacts were removed using signal space projection: cardiac and eye blinks events were identified using default filters in Brainstorm, manually verified, and then used to estimate a small number of basis functions corresponding to these noise components, which were removed from the recordings (Uusitalo and Ilmoniemi, 1997). From these functional data, we extracted two epochs for each trial: (1) a measure of baseline activity (−100 to −1 ms relative to the onset of the first encoding stimulus); and (2) the evoked response (0–4000 ms). We used the baseline measures to estimate the noise covariance for each block and then applied a minimum norm source reconstruction to the evoked data. For each source reconstruction, we used a 15,000 vertex

cortical surface (standard mesh, with atlas information imported from the Freesurfer segmentation). Dipole orientations in the source model were constrained to be normal to the cortical surface, the noise covariance was regularized using the median eigenvalue, and all other options were set to their default values.

ROIs. We defined four ROIs: occipital cortex (OC), ventrotemporal cortex (VTC), PMC, and PFC, based on atlas data aligned with each participant's anatomy during the Freesurfer segmentation process. We used the Destrieux atlas from Freesurfer to define our ROIs (see Destrieux et al., 2010). Our ROIs included the following parcellations from Destrieux et al. (2010, their Table 1): OC included the entire OC (indices 2, 11, 19, 20, 22, 42, 44, 51, 57, 58, 59); VTC included the inferior temporal gyri and sulci (indices 37, 72); PMC included the middle-posterior part of the cingulate gyrus and sulcus, the precuneus, the marginal branch of the cingulate sulcus, and the subparietal sulcus (indices 8, 30, 46, 71); and PFC included the entire PFC (indices 1, 5, 6, 24, 31, 62, 63, 64, 70). These four ROIs are displayed on an uninflated cortical surface in the legend in the top right of Figures 3 and 4. All ROIs comprised continuous parts of the cortical surface: the two separate parts of PMC in these figure legends were joined within the sulcus. For each ROI, we extracted the MEG data corresponding to the subset of the 15,000 sources which were located within the ROI, and used these datasets in the analyses below.

Classification analyses. For each ROI, we performed a series of multivariate pattern classification analyses, within each 5 ms bin across the trial duration. Each classification asked how well the source data from a single ROI in a single time bin could be used to differentiate between trials of two classes: for example, trials with the first encoding stimulus at Location 1 versus Location 2. We trained classifiers (linear support vector machine) to discriminate the location and image of each stimulus (four encoding stimuli + 1 retrieval stimulus): for 9 locations, there were 36 pairwise comparisons; and for 8 images, there were 28 pairwise comparisons. For these classifications, we created "pseudo-trials" by averaging across trials with the same value on the dimension of interest, but with differing values along the other dimension.

Pseudo-trials were always balanced across the irrelevant dimension of interest for the same stimulus. When classifying stimulus location for the first encoding stimulus, each pseudo-trial was the average of 8 trials where the first encoding stimulus was at the same location: one trial of each stimulus image. Similarly, pseudo-trials for classifying stimulus image were balanced across location of that stimulus. To ensure that our results did not depend on a particular assignment on trials to pseudo-trials, we generated 20 sets of pseudo-trials for every pairwise classification, updating the random assignment of trials for each set, and averaged classification performance across these. In each case, we trained the classifier on 90% of the data and tested its performance on the held-out data (10%) to avoid circularity. We repeated this process 10 times (10-fold cross-validation) so that every partition of the pseudo-trials was included in the test set once; then we averaged classifier performance across these.

Since the duration of the stimuli varied across participants (180–320 ms for the encoding stimuli), when averaging classifier accuracy across participants, we first aligned their data at each stimulus onset, meaning that, in Figures 3–6, there are time bins (shaded in gray) where the average includes <11 participants. In these figures, the x axis is labeled for a 320 ms stimulus.

Statistical testing. To evaluate whether classifier performance was significantly above chance, we used a combination of permutation testing and bootstrapping to generate nonparametric null distributions. For each participant, we took the original MEG trial data but randomly shuffled the trial labels across trials within the participant's data. Using this shuffled-label data, we performed the same classification analyses as for the original data, including pseudo-trials and 10-fold cross-validation. We repeated this process 10 times, randomly shuffling the trial labels each time, resulting in 10 estimates of chance-rate classifier performance for each classification at each time. Since this process was computationally intensive, we did not repeat this entire process 10,000 times, but instead we used a Monte Carlo estimation of the distribution (Efron and Tibshirani, 1994), randomly sampling these 10 estimates (with replacement) to generate a sample of 10,000 estimates of each mean for each ROI of each participant. We performed this resampling procedure separately for each pairwise comparison, at each time sample, so that there were different combinations of the original 10 estimates in each case. This resulted in a null distribution of 10,000 datasets against which to compare the observed classifier performance. In the results figures, we plot the range of the central 95% of null values as a gray shaded region along with the results to which they correspond. In each case, we performed all analyses on the null datasets as for the original data (e.g., including averaging across participants) and then sorted the values separately for each time sample; from these, we defined the bounds of the central 95% as the 251st to the 9750th value.

To generate p values, we compared the observed value with the relevant null distribution. For instance, to assess whether classifier performance is above chance (one-sided test), we defined the p value as the proportion of equivalent null means which were above the observed mean (Maris and Oostenveld, 2007). To correct for multiple comparisons across time bins, we applied a false discovery rate (FDR) correction of $q < 0.05$ (Benjamini and Hochberg, 1995) to these p values. In addition to the nonparametric tests based on the null distribution, we used a Bayes factor (BF) analysis: an alternative to the traditional frequentist approach (Kass and Raftery, 1995; Morey and Wagenmakers, 2014) that is increasingly being applied to MEG decoding studies (Teichmann et al., 2021). A BF compares evidence for competing hypotheses; here we report where there is moderate (BF > 3) or strong (BF > 10) evidence in favor of the alternate hypothesis, or at least moderate (BF < 1/3) evidence in favor of the null hypothesis. We implemented all BF analyses using a MATLAB package (Krekelberg, 2021).

Information flow analysis (IFA). From the pairwise classification of each of the 9 locations (36 pairs) and the 8 images (28 pairs), for each of 5 stimuli (4 encoding stimuli and the retrieval stimulus), we had classifier accuracy over time for $(36 + 28) \times 5 = 320$ classifications. Within 5 distinct epochs, corresponding to the time from the presentation of each stimulus until the earliest presentation of the next stimulus (or, in the case of retrieval stimulus, until the end of the trial data), we used the 64 classifier accuracy values from the most recent stimulus as a dissimilarity matrix (*DSM*) at each time bin. We used these DSMs to test for Granger causal relationships between each pair of ROIs (IFA; for this and similar analyses, see Ince et al., 2015; Goddard et al., 2016, 2022; Karimi-Rouzbahani, 2018; Kietzmann et al., 2019). ROI A is said to "Granger cause" the pattern of classification performance in a second ROI (B) if the past of the first ROI can be used to predict future performance of the second ROI better than the past of the second ROI alone. We performed a sliding-window analysis of a simplified (special case) of Granger causality, using the partial correlations (Spearman's ρ) in Equation 2 to define the information flow (IF) from ROI A to ROI B ($IF_{A.B}$) for each time bin (t).

$$IF_{A.B(t,d,w)} = \rho\, DSM_{(B,t)} DSM_{(A,t,d,w)} \cdot DSM_{(B,t,d,w)} \quad (2)$$

where $DSM_{(loc,t)}$ is the *DSM* based on the sources in ROI *loc* at time t ms after stimulus onset, and $DSM_{(loc,t,d,w)}$ is the DSM based on the sources in ROI *loc*, averaged across all time bins from t-d ms to t-$(d + w)$ ms after stimulus onset. We calculated *FF* and *FB* for 30 overlapping windows: for 5 window widths ($w = 10$, 20, 30, 40, or 50 ms) for each of 6 delays ($d = 50$, 60, 70, 80, 90, or 100). As in previous work (Goddard et al., 2022), since the results were broadly similar across values of w and d, we report $IF_{A.B}$ values averaged across all values of w and d.

In addition to reporting $IF_{A.B}$ and $IF_{B.A}$ for each pair of ROIs, we report the difference between these, as shown in Equation 3, to assess the times at which information flow between ROI A and ROI B is dominated by one direction over the other.

$$Diff_{(A.B)} = IF_{A.B} - IF_{B.A} \quad (3)$$

To assess whether each information flow was significantly >0, and whether each difference was significantly different from zero, we repeated the information flow analyses on each of the 10,000 datasets

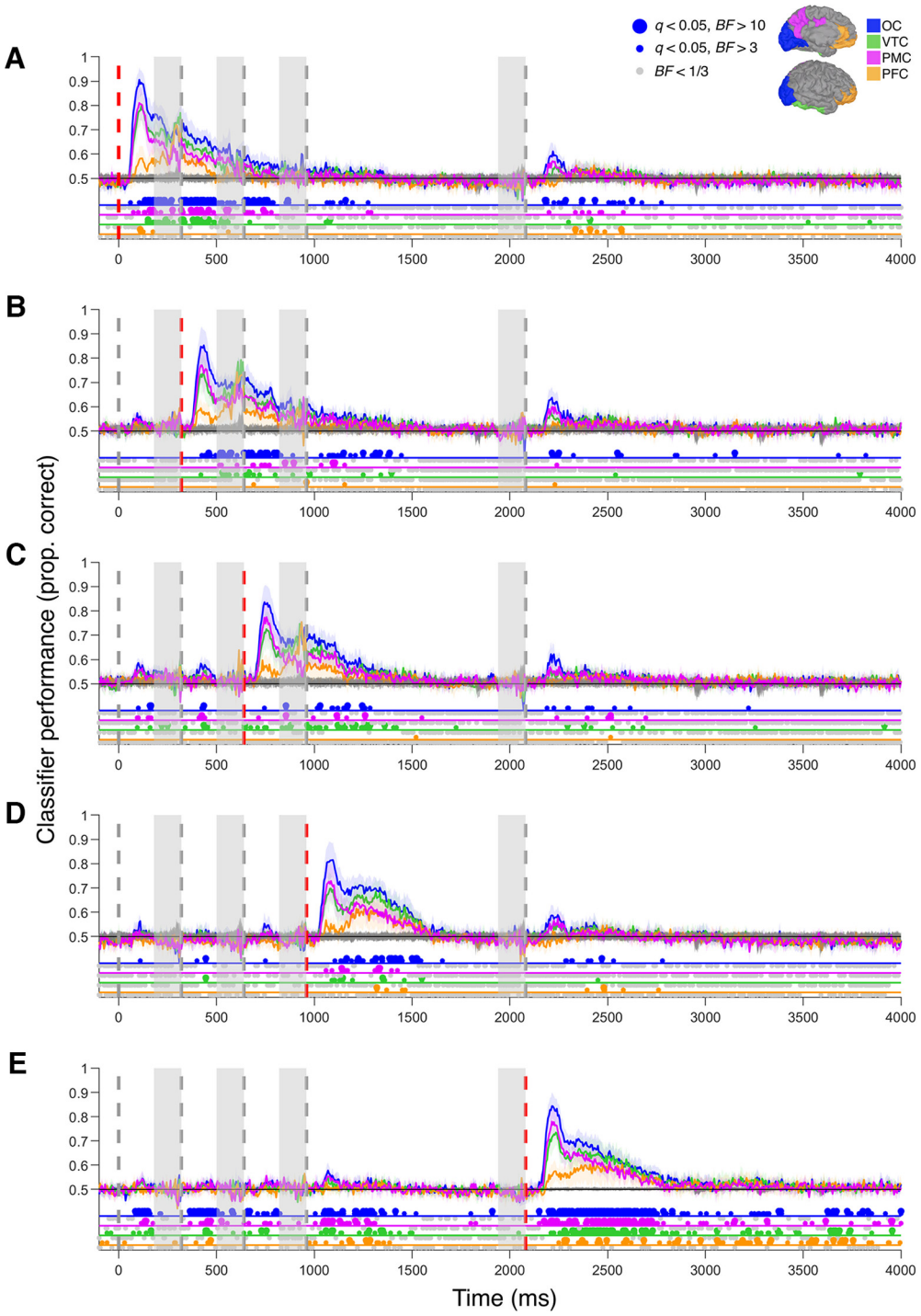

Figure 3. Classifier performance decoding item location, for each of the 4 encoding items (***A–D***) and the retrieval item (***E***), for each ROI. Shaded error bars indicate 95% CIs of the between subject mean ($n = 11$). Shaded gray distribution represents the 95% CIs of a bootstrapped null distribution (see Materials and Methods). Vertical dashed lines indicate the onsets of each stimulus, with the stimulus being decoded highlighted in red in each plot. Shaded regions of the plot represent times where the data are averaged across <11 participants because of the individualized stimulus durations (see Materials and Methods). Dots along the 4 colored lines below the *x* axis represent the statistical results for the data from each ROI. In each case, colored dots above the line represent times where the mean was significantly greater than the bootstrapped null distribution (FDR-corrected, $q < 0.05$), and there was a moderate or strong effect indicated by the BF (BF > 3, small dots, or BF > 10, large dots, respectively). Small gray dots below each line represent times at which there was at least moderate evidence against the presence of above-chance decoding (BF < 1/3). Top right, Legend shows each ROI as a shaded region on an uninflated cortical surface from a medial (top) and lateral (bottom) view.

generated from shuffling trial labels (described above). For each pair of ROIs, this generated null distributions of information flow (*IF*) and differences (*Diff*) against which to compare the observed values. We used these to define the central 95% of the null distribution, in an analogous method to that described above for classifier performance. Similarly, we also obtained *p* values from these null distributions: for *IF*, we asked whether the observed value was greater than the null (one-sided test, as above); and for *Diff*, we asked whether the absolute value of the observed difference was greater in amplitude than the absolute value of the null distribution, defining the *p* value as the proportion of null values with a greater absolute value than the observed (two-sided test). As before, we applied an FDR correction of $q < 0.05$ to these *p* values to correct for

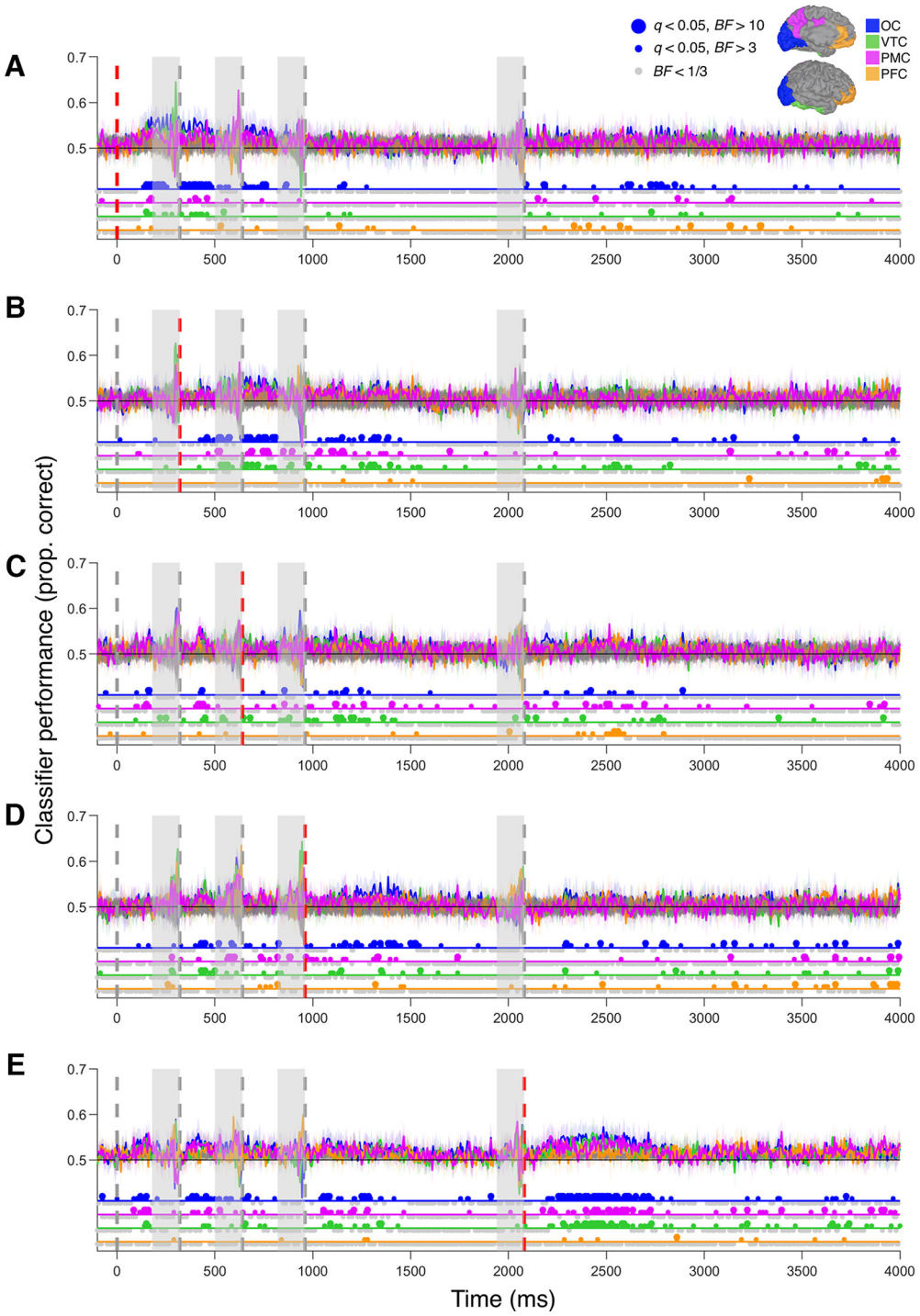

Figure 4. Classifier performance decoding item identity, for each of the 4 encoding items (***A–D***) and the retrieval item (***E***), for each ROI. Plotting conventions as in Figure 3.

multiple comparisons across time points. To complement these analyses, we performed a BF analysis as an index of the relative strength of the observed effects.

Last, we took the average information flow between each pair of ROIs across three functionally relevant epochs, corresponding to the encoding, maintenance, and retrieval task phases, and asked whether the intersubject variability in information flow was correlated with variability in task performance. The "encoding" epoch included the first 180 ms after onset of each of the four encoding stimuli onset, the "maintenance" epoch included the maintenance period from 180 ms after the onset of the fourth encoding stimulus until the earliest onset of the retrieval stimulus, and the "retrieval" epoch corresponded to the onset of the retrieval stimulus until the end of the trial. For the participant with the shortest encoding stimulus duration (180 ms), these three epochs covered the first 3440 ms from the trial onset; while for the participant with the longest encoding stimulus duration (320 ms), the final epoch finished at 4000 ms. Across participants, the median reaction time was 1.99 s after the onset of the retrieval stimulus (lower to upper quartiles: 1.69–2.27 s), meaning that the "retrieval" epoch covered approximately the time until the participant's response. Across each of these epochs, for each pair of ROIs, we averaged data from time points for which there was at least moderate evidence of information flow (i.e., $BF > 3$, $q < 0.05$) in at least

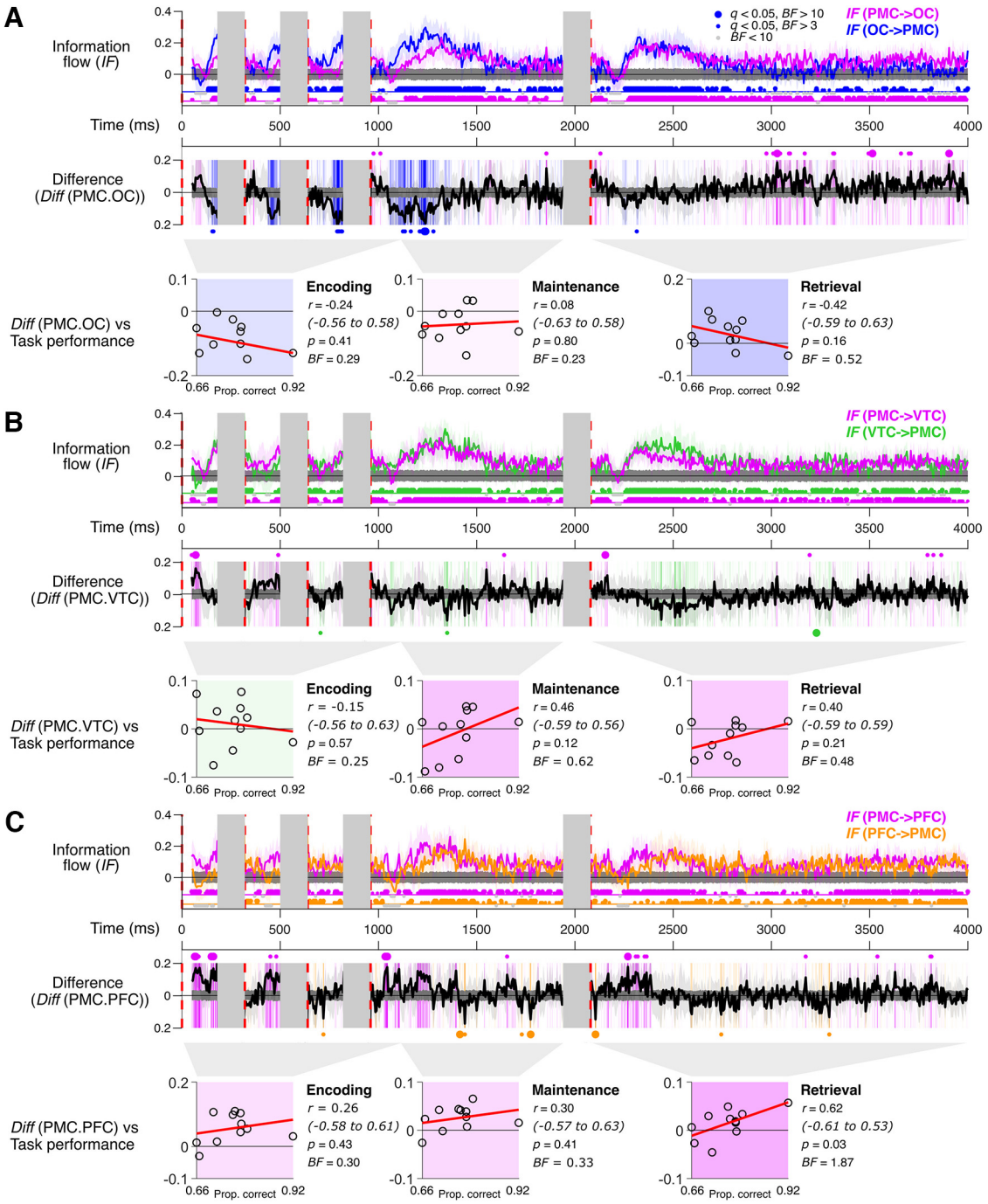

Figure 5. IFA between PMC (magenta) and occipital (***A***, blue), ventrotemporal (***B***, green), and frontal (***C***, orange) cortices. In each case, the uppermost plot represents the information flow to and from PMC to the other area, and the middle plot represents the difference between these information flows. The background of the plot is colored according to the dominant information flow (e.g., darkest magenta represents times of strongest bias from PMC to the other area). Dots below the uppermost plots, and above and below the middle plots represent the BF results. Vertical dashed red lines indicate the onsets of each stimulus; for each time sample, information flow was calculated using classifier decoding of only the most recent stimulus. Shaded regions of the plot represent times where there were data for <11 participants because of the individualized stimulus durations (see Materials and Methods). In the bottom part of each plot, the scatter plots represent the relationship between participant's performance on the task (*d'*) and the information flow bias (*Diff*). For each participant, we calculated their average Diff value by averaging across time samples within the epoch where there was at least a moderate effect (BF > 3) of information flow in at least one direction between the pair (i.e., time samples with at least one colored dot in the uppermost plot). Each scatterplot includes a line of best fit (in red); and beside each correlation plot, the correlation value (Pearson's *r*) is given, along with the range of the central 95% of null *r* values, and the *p* value derived from this null distribution (none of these survived FDR correction at $q < 0.05$). Backgrounds of the scatter plots are colored according to the slope of the line of best fit (e.g., darkest magenta represents the strongest positive relationship between participant performance and information flow from PMC).

one direction between the pair of ROIs. We excluded data from remaining time points to minimize the contribution of data from times where there was weak or no evidence of information flow between the ROIs.

In each case, we report the average difference in information flow ($Diff_{A,B}$), and the linear (Pearson's) correlation (*r*) between participants' average behavioral performance during the MEG session and the average difference in the information flow $Diff_{A,B}$ during the relevant

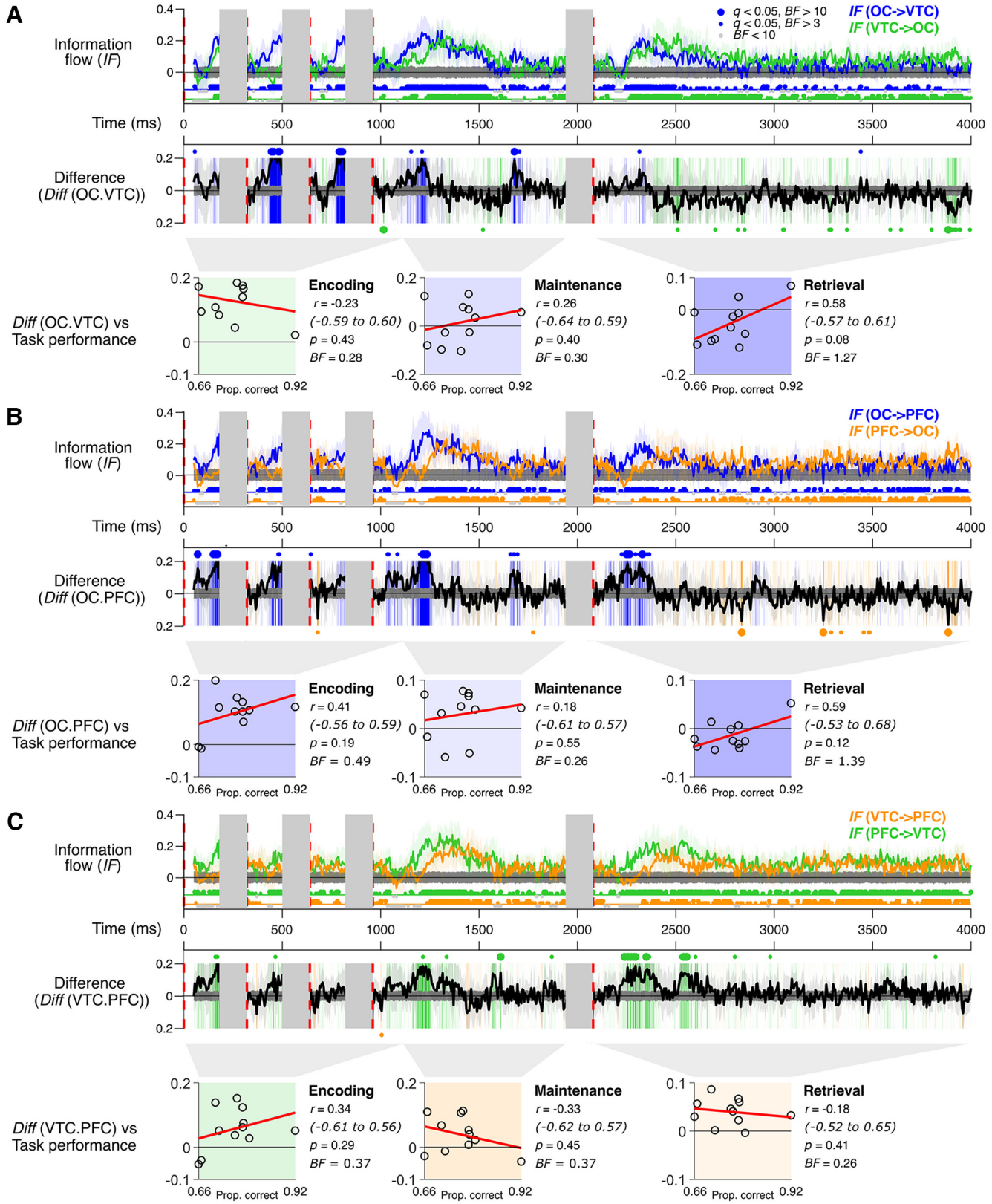

Figure 6. IFA between remaining cortices (excluding PMC). IFA between occipital and ventrotemporal cortices (***A***), occipital and frontal cortices (***B***), and ventrotemporal and frontal cortices (***C***). Plotting conventions are as in Figure 5.

epoch. We repeated this analysis (average $Diff_{A,B}$ and its correlation with behavior) for each of the 10,000 samples of the bootstrapped null data, resulting in a distribution of 10,000 null means and *r* values. As for other results, we report the central 95% of these null values, and we used this null distribution to define *p* values, in this case defining the *p* value as the proportion of null means or *r* values with a greater absolute value than the observed value (two-sided test). Finally, we applied FDR correction to these *p* values to correct for

multiple comparisons across epochs, and calculated the BF for each mean and correlation.

Data availability. Data from MEG experiments are freely available online from the Open Science Framework (https://doi.org/10.17605/OSF.IO/MW3J2). This online repository includes deidentified raw data from the MEG experiments, details of the stimulus timing for each participant, and the MATLAB code used to perform the analyses reported here.

Results

Classification analyses

We used a series of classification analyses to test for times at which the MEG signals in OC, VTC, PMC, and PFC contained information about the location and image of each stimulus during visuospatial working memory performance. Decoding of the location in each stimulus is shown in Figure 3, and decoding of the image at each location is shown in Figure 4. Decoding of stimulus location was higher than decoding of stimulus identity; but for decoding of both location and identity, there was evidence of periods of above-chance decoding of each stimulus in all ROIs.

For decoding stimulus location, we found periods of above-chance decoding of location and identity for each of the four encoding stimuli as well as the retrieval stimulus based on signals from OC, VTC, PMC, or PFC [$q < 0.05$, with FDR correction for multiple comparisons across time bins, including moderate (BF > 3) and strong (BF > 10) effects]. For decoding of stimulus image identity (Fig. 4), we found weaker classifier performance overall, with the proportion correct an order of magnitude lower than for decoding location. Despite the lower overall accuracy, statistical analyses showed that decoding of each stimulus identity was robustly above chance for some time points in all ROIs.

Across all ROIs, the decoding of stimulus location and identity followed a similar evolution over time, with an initial peak, then decay, consistent with signals primarily driven by the visual response to the stimulus. We expected stimulus information in OC to precede that in other ROIs, but the early peaks in decoding in OC, VTC, and PMC occurred at approximately the same time. This suggests that there may be some "signal leakage" between ROIs in our source localization (we return to this question when considering the results of the IFA, below). Nonetheless, the differences between ROIs suggest that these analyses have also captured signals that are nonoverlapping across ROIs. For instance, for decoding stimulus location, the relative accuracy at ~100 ms versus ~300 ms after the onset of the relevant stimulus varies across ROIs.

In Figures 3*A–D* and 4*A–D*, there tends to be a brief period of above-chance decoding during the processing of the retrieval stimulus. It is possible that this reflects some neural process comparing the retrieval stimulus with the remembered locations and identities, especially where this persists to later (e.g., ~300 ms) after the onset of the retrieval stimulus. However, we cannot rule out that decoding at these times could be driven by the neural response to the retrieval stimulus if there is a slight imbalance in the counterbalancing of trials. For instance, brief periods of above-chance decoding before the onset of the relevant stimulus (e.g., around the time of the first encoding stimulus in Figs. 3*B–E* and 4*B–E*) clearly cannot be driven by a response to the decoded stimulus. This may have arisen since each trial was defined to include four different locations and four different identities during encoding; so, for example, decoding Location 1 versus Location 3 for encoding Stimulus 2 is equivalent to decoding "not Location 1" versus "not Location 3" for other encoding stimuli. Either way, our results suggest that signals based on remembered stimulus locations or identities were very weak compared with the robust signals comprising the visually driven response.

IFA

We next considered Granger-causal interactions between each pair of ROIs using an IFA. Even when classifier performance is low, overall there may be small, genuine signals that drive differences in the pattern of classifier performance across the many different pairwise classifications for each time bin. However, to ensure our measures of information flow were not driven by any spurious effects, we performed this analysis using classifications of only the most recent stimulus for each trial epoch (see Materials and Methods). IFA specifically tests for differences between ROIs and the temporal structure of these differences, rendering it potentially more sensitive than average classifier performance for detecting differences between ROIs. The results of our IFAs between PMC and all other ROIs are shown in Figure 5, with interactions between the remaining ROIs shown in Figure 6.

The IFAs revealed periods of significant Granger-causal interactions between each pair of ROIs [$q < 0.05$, with FDR correction, including times of moderate (BF > 3) and strong (BF > 10) effects] across all trial phases (encoding, maintenance, and retrieval). The information flows (uppermost plots in each case for Figs. 5 and 6) were strongest in each direction near periods of higher classifier performance; but within each pair of ROIs, the relative strength of each ROI in influencing the other varied over time, as reflected in the difference plots. When OC was paired with any other ROI, information flow from OC tended to be higher than information flow to OC immediately after each stimulus onset, consistent with a stimulus-driven response. This was particularly pronounced for the encoding epoch, where average difference in information flow between OC and any other ROI ($avg\ Diff_{OC.\times}$) varied from 0.094 to 0.127, and the BF indicated a series of strong effects in favor of greater information flow from OC to the other area ($q < 0.05$, BF > 10 in each case). There was also a moderate effect of information flow from OC to PMC exceeding the reverse direction during maintenance ($avg\ Diff_{OC.PMC} = 0.042$, $q < 0.05$, BF = 3.19).

We were particularly interested in whether there was evidence of information flow from PMC shaping responses in other areas. The strongest evidence for this was between PMC and PFC. Average information flow from PMC to PFC tended to exceed the reverse direction over all epochs, with a strong effect during encoding ($avg\ Diff_{PMC.PFC} = 0.056$, $q < 0.05$, BF = 18.70), and a moderate effect during maintenance ($avg\ Diff_{PMC.PFC} = 0.025$, $q < 0.05$, BF = 7.33), but this bias did not reach significance during retrieval ($avg\ Diff_{PMC.PFC} = 0.014$, $q > 0.05$, BF = 0.77). The time courses in Figure 5*C* show that, across all trial epochs, information flow from PMC to PFC was strongest around the time of the early, stimulus-driven response to each stimulus. With OC, PMC showed evidence of greater information flow in the latter part of the retrieval epoch (Fig. 5*A*). Averaged across the retrieval epoch, this difference was biased toward PMC driving OC, but this was a small effect ($avg\ Diff_{PMC.PFC} = 0.029$, $q < 0.05$, BF = 1.59).

Across remaining ROI pairs, the only cases with a moderate or greater effect (BF > 3) were between VT and PFC (Fig. 6*C*), during encoding ($avg\ Diff_{VT.PFC} = 0.057$, $q < 0.05$, BF = 4.00) and retrieval ($avg\ Diff_{VT.PFC} = 0.040$, $q < 0.05$, BF = 57.79). As for OC, the times where VT dominated information flow with PFC were consistent with the early stimulus-driven response (e.g., compare times of dominance of VT in Fig. 6*C* and OC in Fig. 6*B*). Overall,

there was little evidence of PFC dominating information flow to other areas.

Last, for each trial epoch, we correlated the average information flow between each pair of ROIs with behavioral accuracy across participants. None of these correlations reached statistical significance once corrected for multiple comparisons, and no correlation reached the level of a moderate effect (BF > 3). This suggests that our relatively small sample size was insufficient to detect any predictive power of information flow for task performance. However, we believe such correlations could be a fruitful direction for future research adopting these methods, so we include these preliminary results as reference for future work.

Discussion

Despite the demonstrated importance of the PMC during memory retrieval, the causal influence of PMC over other regions has remained unclear. Specifically, the direction and content of information exchange between PMC and other brain regions during memory processes have not been tested. Here, we used MEG recordings from MRI-defined ROIs to evaluate information flow between PMC and other regions during a visuospatial working memory task. Results suggest that PMC object representations show Granger-causal influence on stimulus information in other regions, most notably in its influence on PFC across all task phases. There was also the suggestion that PMC shapes responses in OC during retrieval.

PMC shapes stimulus representations in prefrontal areas

Our most striking finding concerns the influence of PMC on remembered stimulus information in PFC. Across all task phases, information flow from PMC to PFC tended to be more dominant than the reverse direction. Since our measure of information flow is based on classification performance, rather than response amplitude, this finding suggests that the stimulus-related information in PMC was predictive of stimulus representations that were about to emerge in PFC. This was most evident for the encoding and maintenance phases; however, PMC was also found to shape responses in PFC during the retrieval phase. The fact that this effect occurred shortly after the retrieval stimulus onset resonates with PMC relaying information on which the participant's decision is based, to PFC to support successful recall.

Prefrontal regions are reliably implicated in attentional control and the flexible coding of task-relevant information (Duncan, 2010; Freedman and Assad, 2016). Patterns of anatomic connectivity between the hippocampus and frontal visuo-oculomotor systems (i.e., dorsolateral PFC and frontal eye fields) (Shen et al., 2016) suggest that frontal regions are particularly well situated to integrate visual memory information to guide behavior (Conti and Irish, 2021). The frontoparietal regions implicated in attentional control are also involved in working memory, especially during encoding and maintenance periods (Gazzaley and Nobre, 2012). Additionally, prefrontal regions are known to drive changes in visual cortex; for instance, microstimulation of the frontal eye fields produces changes in visual cortex consistent with shifts of attention (Moore et al., 2003; Premereur et al., 2013).

Our results suggest that PMC shapes prefrontal representations of remembered visuospatial information throughout task performance and including the beginning of the retrieval period. Previous fMRI work has demonstrated increased frontoparietal activation during encoding and maintenance whether retrieval was required or not, while posterior cingulate cortex showed response patterns consistent with a role in retrieval (Rahm et al., 2014). Functional connectivity between PMC and prefrontal regions, such as ventromedial PFC, lends further support to the importance of frontoparietal coupling during episodic retrieval (for review, see Andrews-Hanna, 2012; Ritchey and Cooper, 2020). Our findings extend previous work by suggesting that this observed pattern of connectivity includes PMC influencing task-relevant information in prefrontal networks.

As with any correlation, it is possible that our partial correlations in the IFA reflect associations with another (untested) area. Another possibility is that our ROIs were not fully isolated during source reconstruction and include signals from nearby regions. If PMC signals were present in the PFC ROI or vice versa, this would increase the shared variance between the ROIs. Shared variance might reduce the extent to which signals in one ROI contribute information above that already present in the other ROI, which could decrease the measured information flow.

PMC influences early sensory cortex during retrieval

Our results further suggest that, during retrieval, PMC shapes responses in sensory cortex. Across all task phases, and for each ROI pairing, the OC tended to dominate information flow, influencing other regions more than it was influenced by these regions, consistent with the visual nature of the task. However, the dominance of OC in our measures of information flow may have been amplified by the generally transient classifier performance observed. Across all ROIs, above-chance decoding was largely restricted to brief epochs after the stimulus presentations, suggesting that any neural representation of the maintained information made minimal contribution to classifier performance. Notably, we found some evidence of significant information flow from PMC to OC in the latter part of the retrieval period (BF = 1.59). Whether this information flow is functionally relevant remains unclear. Any functional influence of PMC on OC must be mediated by indirect connections, since there are no direct projections between PMC and primary sensorimotor regions (Parvizi et al., 2006; Leech and Smallwood, 2019). Candidate indirect pathways by which PMC could influence occipital regions include the parieto-medial temporal pathway, which is proposed to contribute to visuospatial processing (Kravitz et al., 2011).

Implications for understanding PMC function

Overall, our results suggest that the PMC has a specific role in relaying stimulus-related information to other regions. This then begs the question of what exactly the PMC is doing. While our results suggest a directionality of PMC influence to other brain regions, the precise function of the PMC in this context remains unclear. The PMC represents one of the major hubs of the brain's default mode network, defined by its "task negative" response profile (Buckner et al., 2005). However, we demonstrate here that PMC does not show a simple task negative contribution to visuospatial memory. PMC engagement during encoding and maintenance is associated with poorer task performance (Piccoli et al., 2015; Santangelo and Bordier, 2019), yet the PMC "encoding/retrieval flip" suggests that increased activity during retrieval is associated with better recall (Daselaar et al., 2004, 2009). While activity alone may reflect content-unspecific contributions, our measures of stimulus representations, using classifier performance, suggest that PMC actively shapes representations of stimulus-related information in other regions during task performance. Accordingly, PMC is not engaged in the processing of purely

external sensory stimuli, but actively involved in the representation of internal content, including remembered information (Leech and Smallwood, 2019). Our study, however, was underpowered to delineate how information flow between PMC and other brain regions is predictive of behavioral accuracy, and we suggest this will be a critical avenue to explore in future work.

Future directions

As the first study, to our knowledge, to explore the exchange of stimulus-related information between PMC and other regions, our study raises several directions for future research. While we focused here on four *a priori* ROIs, and used a relatively small sample size, it will be important to comprehensively map the flow of information between PMC and other brain regions during visuospatial memory with larger cohorts of participants. Time-resolved methods, such as MEG/EEG, could also be complemented with imaging methods, such as fMRI, to test finer parcellations within these regions.

We had low overall decoding during maintenance, and so, a limited ability to detect information flow during this task phase. We chose visually similar stimuli to increase task difficulty and reduce verbal labeling. However, this may have decreased classifier performance for task identity. Decoding was higher for stimulus location, where the retinotopic organization of visual cortical areas would yield larger-spatial scale response differences, yet even for location, beyond the stimulus-induced response, we found little evidence of decoding based on remembered values. Conversely, in decoding EEG signals during a simpler visual memory task, Bocincova and Johnson (2019) report above-chance decoding of stimuli during a delay period, albeit weaker than during encoding. Thus, while high task difficulty appears necessary to isolate the specific role of the PMC (Kochan et al., 2011; Leech et al., 2011; Vannini et al., 2011), a less demanding task might yield better classifier performance, to better detect information flows across all task phases.

Efforts to delineate the functional relevance of PMC subregions may also offer crucial insights into the early and accurate diagnosis of Alzheimer's disease (Buckner et al., 2005; Xia et al., 2014; Wu et al., 2016; Khan et al., 2020). Emerging evidence suggests that healthy young adults carrying the APOE-ε4 allele exhibit inefficiencies modulating PMC activity during scene (but not face and object) working memory and perception (e.g., Shine et al., 2015), while functional deactivation of PMC during visuospatial working memory performance is predictive of subsequent cognitive decline in older adults with mild cognitive impairment (Kochan et al., 2011). Given that visuospatial dysfunction because of PMC dysfunction has been proposed as an early harbinger of Alzheimer's disease (Pihlajamäki et al., 2010; Irish et al., 2012; Salimi et al., 2018), future studies investigating functional changes in the PMC may improve the early identification of individuals at risk of dementia.

References

Andrews-Hanna JR (2012) The brain's default network and its adaptive role in internal mentation. Neuroscientist 18:251–270.

Benjamini Y, Hochberg Y (1995) Controlling the false discovery rate: a practical and powerful approach to multiple testing. J R Stat Soc Ser B Methodol 57:289–300.

Bird CM, Keidel JL, Ing LP, Horner AJ, Burgess N (2015) Consolidation of complex events via reinstatement in posterior cingulate cortex. J Neurosci 35:14426–14434.

Bocincova A, Johnson JS (2019) The time course of encoding and maintenance of task-relevant versus irrelevant object features in working memory. Cortex 111:196–209.

Brainard DH (1997) The Psychophysics Toolbox. Spat Vis 10:433–436.

Buckner RL, Snyder AZ, Shannon BJ, LaRossa G, Sachs R, Fotenos AF, Sheline YI, Klunk WE, Mathis CA, Morris JC, Mintun MA (2005) Molecular, structural, and functional characterization of Alzheimer's disease: evidence for a relationship between default activity, amyloid, and memory. J Neurosci 25:7709–7717.

Bzdok D, Heeger A, Langner R, Laird AR, Fox PT, Palomero-Gallagher N, Vogt BA, Zilles K, Eickhoff SB (2015) Subspecialization in the human posterior medial cortex. Neuroimage 106:55–71.

Canolty RT, Edwards E, Dalal SS, Soltani M, Nagarajan SS, Kirsch HE, Berger MS, Barbaro NM, Knight RT (2006) High gamma power is phase-locked to theta oscillations in human neocortex. Science 313:1626–1628.

Conti F, Irish M (2021) Harnessing visual imagery and oculomotor behaviour to understand prospection. Trends Cogn Sci 25:272–283.

Cooper RA, Ritchey M (2019) Cortico-hippocampal network connections support the multidimensional quality of episodic memory. Elife 8:e45591.

Dale AM, Fischl B, Sereno MI (1999) Cortical surface-based analysis: I. Segmentation and surface reconstruction. Neuroimage 9:179–194.

Daselaar SM, Prince SE, Cabeza R (2004) When less means more: deactivations during encoding that predict subsequent memory. Neuroimage 23:921–927.

Daselaar SM, Prince SE, Dennis NA, Hayes SM, Kim H, Cabeza R (2009) Posterior midline and ventral parietal activity is associated with retrieval success and encoding failure. Front Hum Neurosci 3:13.

Destrieux C, Fischl B, Dale A, Halgren E (2010) Automatic parcellation of human cortical gyri and sulci using standard anatomical nomenclature. Neuroimage 53:1–15.

Duncan J (2010) The multiple-demand (MD) system of the primate brain: mental programs for intelligent behaviour. Trends Cogn Sci 14:172–179.

Efron B, Tibshirani RJ (1994) An introduction to the bootstrap. New York: Chapman and Hall/CRC.

Fell J, Axmacher N (2011) The role of phase synchronization in memory processes. Nat Rev Neurosci 12:105–118.

Fischl B, Sereno MI, Dale AM (1999) Cortical surface-based analysis: II. Inflation, flattening, and a surface-based coordinate system. Neuroimage 9:195–207.

Freedman DJ, Assad JA (2016) Neuronal mechanisms of visual categorization: an abstract view on decision making. Annu Rev Neurosci 39:129–147.

Fuentemilla L, Barnes GR, Düzel E, Levine B (2014) Theta oscillations orchestrate medial temporal lobe and neocortex in remembering autobiographical memories. Neuroimage 85:730–737.

Gazzaley A, Nobre AC (2012) Top-down modulation: bridging selective attention and working memory. Trends Cogn Sci 16:129–135.

Goddard E, Carlson TA, Dermody N, Woolgar A (2016) Representational dynamics of object recognition: feedforward and feedback information flows. Neuroimage 128:385–397.

Goddard E, Carlson TA, Woolgar A (2022) Spatial and feature-selective attention have distinct, interacting, effects on population-level tuning. J Cogn Neurosci 34:290–312.

Huang MX, Mosher JC, Leahy RM (1999) A sensor-weighted overlapping-sphere head model and exhaustive head model comparison for MEG. Phys Med Biol 44:423–440.

Huijbers W, Vannini P, Sperling RA, Pennartz CM, Cabeza R, Daselaar SM (2012) Explaining the encoding/retrieval flip: memory-related deactivations and activations in the posteromedial cortex. Neuropsychologia 50:3764–3774.

Huijbers W, Schultz AP, Vannini P, McLaren DG, Wigman SE, Ward AM, Hedden T, Sperling RA (2013) The encoding/retrieval flip: interactions between memory performance and memory stage and relationship to intrinsic cortical networks. J Cogn Neurosci 25:1163–1179.

Hunsaker MR, Kesner RP (2018) Unfolding the cognitive map: the role of hippocampal and extra-hippocampal substrates based on a systems analysis of spatial processing. Neurobiol Learn Mem 147:90–119.

Ince RA, van Rijsbergen NJ, Thut G, Rousselet GA, Gross J, Panzeri S, Schyns PG (2015) Tracing the flow of perceptual features in an algorithmic brain network. Sci. Rep 5:17681.

Irish M, Piguet O, Hodges JR (2012) Self-projection and the default network in frontotemporal dementia. Nat Rev Neurol 8:152–161.

Kado H, Higuchi M, Shimogawara M, Haruta Y, Adachi Y, Kawai J, Ogata H, Uehara G (1999) Magnetoencephalogram systems developed at KIT. IEEE Trans Appl Supercond 9:4057–4062.

Karimi-Rouzbahani H (2018) Three-stage processing of category and variation information by entangled interactive mechanisms of peri-occipital and peri-frontal cortices. Sci Rep 8:12213.

Kass RE, Raftery AE (1995) Bayes factors. J Am Stat Assoc 90:773–795.

Kernbach JM, Yeo BT, Smallwood J, Margulies DS, Thiebaut de Schotten M, Walter H, Sabuncu MR, Holmes AJ, Gramfort A, Varoquaux G, Thirion B, Bzdok D (2018) Subspecialization within default mode nodes characterized in 10,000 UK Biobank participants. Proc Natl Acad Sci USA 115:12295–12300.

Khan W, Amad A, Giampietro V, Werden E, De Simoni S, O'Muircheartaigh J, Westman E, O'Daly O, Williams SC, Brodtmann A, Alzheimer's Disease Neuroimaging Initiative (2020) The heterogeneous functional architecture of the posteromedial cortex is associated with selective functional connectivity differences in Alzheimer's disease. Hum Brain Mapp 41: 1557–1572.

Kietzmann TC, Spoerer CJ, Sörensen LK, Cichy RM, Hauk O, Kriegeskorte N (2019) Recurrence is required to capture the representational dynamics of the human visual system. Proc Natl Acad Sci USA 116:21854–21863.

Kleiner M, Brainard D, Pelli DG (2007) What's new in Psychtoolbox-3? Perception 36 ECVP Abstract Supplement.

Kochan NA, Breakspear M, Slavin MJ, Valenzuela M, McCraw S, Brodaty H, Sachdev PS (2010) Functional alterations in brain activation and deactivation in mild cognitive impairment in response to a graded working memory challenge. Dement Geriatr Cogn Disord 30:553–568.

Kochan NA, Breakspear M, Valenzuela M, Slavin MJ, Brodaty H, Wen W, Trollor JN, Turner A, Crawford JD, Sachdev PS (2011) Cortical responses to a graded working memory challenge predict functional decline in mild cognitive impairment. Biol Psychiatry 70:123–130.

Kravitz DJ, Saleem KS, Baker CI, Mishkin M (2011) A new neural framework for visuospatial processing. Nat Rev Neurosci 12:217–230.

Krekelberg B (2021) klabhub/bayesFactor: ttest updates. Zenodo.

Leech R, Braga R, Sharp DJ (2012) Echoes of the brain within the posterior cingulate cortex. J Neurosci 32:215–222.

Leech R, Kamourieh S, Beckmann CF, Sharp DJ (2011) Fractionating the default mode network: distinct contributions of the ventral and dorsal posterior cingulate cortex to cognitive control. J Neurosci 31:3217–3224.

Leech R, Smallwood J (2019) The posterior cingulate cortex: insights from structure and function. Handb Clin Neurol 166:73–85.

Lega B, Germi J, Rugg M (2017) Modulation of oscillatory power and connectivity in the human posterior cingulate cortex supports the encoding and retrieval of episodic memories. J Cogn Neurosci 29:1415–1432.

Margulies DS, Vincent JL, Kelly C, Lohmann G, Uddin LQ, Biswal BB, Villringer A, Castellanos FX, Milham MP, Petrides M (2009) Precuneus shares intrinsic functional architecture in humans and monkeys. Proc Natl Acad Sci USA 106:20069–20074.

Maris E, Oostenveld R (2007) Nonparametric statistical testing of EEG- and MEG-data. J Neurosci Methods 164:177–190.

Moore T, Armstrong KM, Fallah M (2003) Visuomotor origins of covert spatial attention. Neuron 40:671–683.

Morey RD, Wagenmakers EJ (2014) Simple relation between Bayesian order-restricted and point-null hypothesis tests. Stat Prob Lett 92:121–124.

Natu VS, Lin JJ, Burks A, Arora A, Rugg MD, Lega B (2019) Stimulation of the posterior cingulate cortex impairs episodic memory encoding. J Neurosci 39:7173–7182.

Parvizi J, Van Hoesen GW, Buckwalter J, Damasio A (2006) Neural connections of the posteromedial cortex in the macaque. Proc Natl Acad Sci USA 103:1563–1568.

Pelli DG (1997) The VideoToolbox software for visual psychophysics: transforming numbers into movies. Spat Vis 10:437–442.

Piccoli T, Valente G, Linden DE, Re M, Esposito F, Sack AT, Di Salle F (2015) The default mode network and the working memory network are not anti-correlated during all phases of a working memory task. PLoS One 10:e0123354.

Pihlajamäki M, O'Keefe K, Bertram L, Tanzi RE, Dickerson BC, Blacker D, Albert MS, Sperling RA (2010) Evidence of altered posteromedial cortical FMRI activity in subjects at risk for Alzheimer disease. Alzheimer Dis Assoc Disord 24:28–36.

Premereur E, Janssen P, Vanduffel W (2013) FEF-microstimulation causes task-dependent modulation of occipital fMRI activity. Neuroimage 67:42–50.

Rahm B, Kaiser J, Unterrainer JM, Simon J, Bledowski C (2014) fMRI characterization of visual working memory recognition. Neuroimage 90:413–422.

Ritchey M, Cooper RA (2020) Deconstructing the posterior medial episodic network. Trends Cogn Sci 24:451–465.

Salimi S, Irish M, Foxe D, Hodges JR, Piguet O, Burrell JR (2018) Can visuospatial measures improve the diagnosis of Alzheimer's disease? Alzheimers Dement (Amst) 10:66–74.

Santangelo V, Bordier C (2019) Large-scale brain networks underlying successful and unsuccessful encoding, maintenance, and retrieval of everyday scenes in visuospatial working memory. Front Psychol 10:233.

Sauseng P, Peylo C, Biel AL, Friedrich EV, Romberg-Taylor C (2019) Does cross-frequency phase coupling of oscillatory brain activity contribute to a better understanding of visual working memory? Br J Psychol 110:245–255.

Shen K, Bezgin G, Selvam R, McIntosh AR, Ryan JD (2016) An anatomical interface between memory and oculomotor systems. J Cogn Neurosci 28:1772–1783.

Shine JP, Hodgetts CJ, Postans M, Lawrence AD, Graham KS (2015) APOE-ε4 selectively modulates posteromedial cortex activity during scene perception and short-term memory in young healthy adults. Sci Rep 5:16322.

Tadel F, Baillet S, Mosher JC, Pantazis D, Leahy RM (2011) Brainstorm: a user-friendly application for MEG/EEG analysis. Comput Intell Neurosci 2011:879716.

Teichmann L, Moerel D, Baker C, Grootswagers T (2021) An empirically-driven guide on using Bayes factors for M/EEG decoding. bioRxiv. doi:10.1101/2021.06.23.449663.

Uehara G, Adachi Y, Kawai J, Shimogawara M, Higuchi M, Haruta Y, Ogata H, Kado H (2003) Multi-channel SQUID systems for biomagnetic measurement. IEICE Trans Electron E86C:43–54.

Uusitalo MA, Ilmoniemi RJ (1997) Signal-space projection method for separating MEG or EEG into components. Med Biol Eng Comput 35:135–140.

Vannini P, O'Brien J, O'Keefe K, Pihlajamäki M, Laviolette P, Sperling RA (2011) What goes down must come up: role of the posteromedial cortices in encoding and retrieval. Cereb Cortex 21:22–34.

Wu Y, Zhang Y, Liu Y, Liu J, Duan Y, Wei X, Zhuo J, Li K, Zhang X, Yu C, Wang J, Jiang T (2016) Distinct changes in functional connectivity in posteromedial cortex subregions during the progress of Alzheimer's disease. Front Neuroanat 10:41.

Xia M, Wang Z, Dai Z, Liang X, Song H, Shu N, Li K, He Y (2014) Differentially disrupted functional connectivity in posteromedial cortical subregions in Alzheimer's disease. J Alzheimers Dis 39:527–543.